Research on Design and Topology Optimization of Personalized Scoliosis Orthopedic Device

Jiahong Liu, Li Wu*, Lei Lei, Ping Gao

Institute of Mechanical Engineering, Dalian Jiaotong University, Dalian 116028, China

Abstract: The incidence of adolescent idiopathic scoliosis (AIS) is on the rise. Clinically, conservative treatment usually involves wearing spinal orthoses. However, traditional orthoses are bulky, which adversely affects patient tolerance and quality of life. Therefore, the development of personalized, lightweight spinal orthoses that also take into account mechanical performance holds significant practical value. Based on 3D-scanned trunk data, the designs of the iliac crest, three-point force application areas, and relief zones are completed through deviation analysis and X-ray-model registration. A finite element model is established to simulate the mechanical responses under two states: wearing the orthosis and applying an opening force. By comparing four material removal rate schemes, the "50% material removal scheme" is identified as the optimal initial-stage scheme. Based on the optimization results, the left iliac crest is further selected as the optimization area for secondary topological optimization. The results show that the secondary topological optimization achieves an additional 6.7% weight reduction compared to the "50% material removal scheme," resulting in a total weight reduction of 41.6%. The maximum stress is 46.63 MPa, and the maximum deformation in the orthotic region is 0.74 mm, both of which meet the design requirements. This study provides a reference for the lightweight design of spinal orthoses for patients with specific types of scoliosis.

Keywords: Scoliosis; Orthosis; Lightweight; Topological Optimization; Reverse Engineering

DOI: 10.57237/j.wjcm.2025.04.001

1 Introduction

Scoliosis is a three-dimensional deformity of the spine [1], encompassing curvature deformations in both the sagittal and coronal planes, as well as torsional deformations in the axial plane, accompanied by rib and pelvic obliquity. The Cobb method is used to measure the scoliosis angle on standing anteroposterior spinal radiographs, and clinically, a scoliosis angle greater than 10° is defined as scoliosis [2].

Treatment approaches for scoliosis are categorized into surgical and non-surgical interventions [3], with non-surgical treatments accounting for approximately 90% of cases [4]. Wearing a scoliosis orthosis represents an effective non-surgical treatment option [5], enabling patients to reduce the degree of scoliosis through orthotic use [6]. Although spinal orthoses can clinically improve scoliosis, issues such as low tolerance due to excessive pressure during wear persist. Therefore, it is necessary to optimize the orthosis layout using finite element methods [7] to reduce weight while ensuring mechanical performance. Iason Rossetos [8] and colleagues demonstrated that increasing the thickness of key orthosis regions could achieve lightweight design without compromising strength. Liao Yiqing [9] and colleagues, incorporating patient Cobb angle assessments, confirmed that optimized braces maintained corrective efficacy while reducing weight. Nikita Cobetto [10] and colleagues employed fi-

Funding: Natural Science Foundation of Liaoning Province (Grant No. LJKMZ20220841).

*Corresponding author: Li Wu, djtuwuli@163.com

Received: 29 November 2025; Accepted: 25 December 2025; Published Online: 30 December 2025 http://www.wjclinmed.com

nite element modeling and 3D reconstruction design methods to achieve material reduction in orthoses, with clinical comparisons showing that the lightweight orthoses exhibited better corrective outcomes. In other orthotic fields, Tz-How H [11] and colleagues reduced the weight of a thumb orthosis through finite element analysis, identifying 3.2 mm as the optimal thickness and achieving a 35% volume reduction. S F Khan [12] and colleagues performed topological optimization on an ankle-foot orthosis, resulting in a 22.56% reduction in stress and a 4.33% reduction in volume.

While existing studies have validated the feasibility of finite element simulation and topological optimization for material reduction in orthoses, research on multi-condition force simulation and multi-scheme validation comparisons for personalized orthoses remains insufficient. Therefore, this study aims to achieve weight reduction in personalized orthoses by employing optimization methods based on multi-condition force simulation and multi-scheme analysis.

2 3D Model of the Human Body's External Contour

The patient wore an elastic vest, and the clavicles, anterior superior iliac spines (ASIS), and posterior superior iliac spines (PSIS) were identified and marked with adhesive tape by medical staff. The patient's information is presented in Table 1.

Table 1 Patient Information

Item	Details
Age	14 years old
Gender	Male
Height/ cm	170
Weight/ kg	41
Three Circumferences	Chest: 67 cm, Waist: 57 cm, Hips: 77 cm
Scoliosis Angle/ °	19 °(measured by Cobb method)
Scoliosis Type	Thoracolumbar single curve with kyphosis

A portable 3D scanner from Occipital was used to capture the patient's body contour features and export the trunk contour point cloud data. In Geomagic software, the point cloud data was fitted into a surface model, and optimal-fit alignment was performed with the point cloud data as the reference. The maximum deviation between the two was found to be 0.16 mm, with an average deviation of 0.016 mm, both of which are below the preset threshold of 0.2 mm [13]. The model accuracy meets the requirements for reverse engineering design.

3 Establishment of the Orthosis Model

3.1 Matching X-ray Images with the Human Body Model

The human body STL file was imported into Blender software, followed by the insertion of the patient's standing anteroposterior (AP) and lateral X-ray images. The positions of the X-rays and the 3D model were spatially aligned, after which the trunk region—spanning from the clavicles to the greater trochanters—was cropped and retained. The arms were trimmed at the shoulder level. (The matching of X-ray images with the fitted model is illustrated in Figure 1).

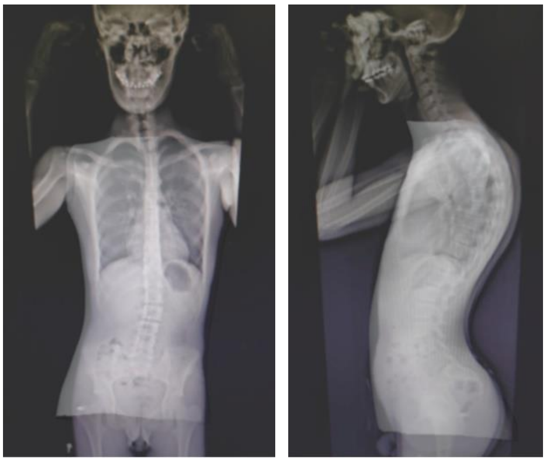

Figure 1 X-ray Image and Fitted Model Matching Diagram

3.2 Design of the Iliac Crest Region

The design conforms to the physiological anatomical contour above the iliac crest, incorporating an ellipsoidal indentation directed inward toward the human body. The normal range for indentation depth is 20–40 mm. Considering the patient's individual parameters (height: 170 cm, weight: 41 kg, BMI: 14.2, classified as underweight), the indentation depth was reduced to 25 mm. The ellipsoid measures 90 mm in length, with a maximum width of 30 mm, and its three principal diameters are 90 mm, 30 mm, and 25 mm, respectively. The modification effect on the iliac crest is detailed in Figure 2a.

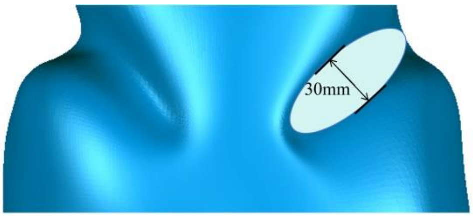

a. Schematic Representation of Iliac Crest Modification

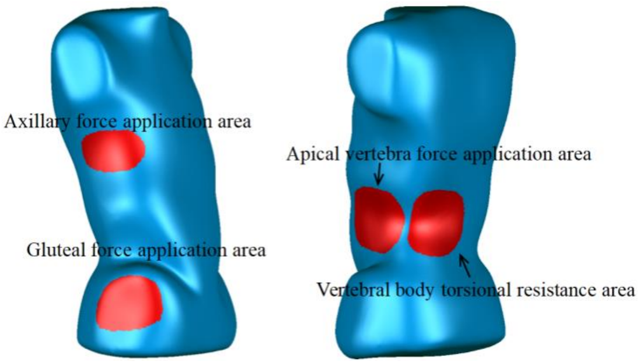

b. Schematic Representation of the Force Application Zone

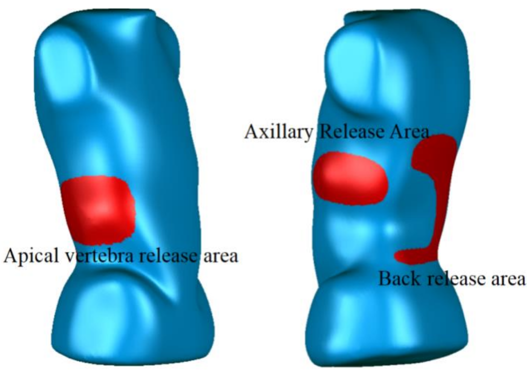

c. Schematic Representation of the Pressure-Relief Zone

Figure 2 Schematic Diagram of the Orthosis Iliac Crest and Correction Zones

3.3 Force Application Zone Design

The patient's X-ray shows unilateral scoliosis, with the apical vertebra located in the thoracolumbar region between T12-L1. The Cobb angle measures 19°, Risser sign is Grade III, and according to the Nash-Moe method, there is also Grade II vertebral rotation [14].

Based on the three-point force principle, a corrective force is applied at the apical vertebra of the patient, while two types of balancing support forces are set on the contralateral side relative to the apical vertebra. Additionally, to address vertebral torsion, a tangential counteracting force for torsion is applied on the lateral side of the back corresponding to the scoliosis, with the application range shown in Figure 2b.

1) Apical vertebra: Combining the patient's X-ray and using geometric projection methods, it is determined that the apical vertebra of the patient deviates approximately 16 mm from the body's midline. Along the rib direction, an indentation distance of 9 mm is applied to the human body according to the standard that the initial corrective indentation distance at the apical vertebra should be 50%-60% of the spinal deviation [15], and also considering the patient's body type. The depth gradually decreases from the force application center to the edges. The indentation shapes at the other two positions are the same, with the range covering the upper and lower end vertebrae, namely T10-L4.
2) Axilla: A force is applied along the rib direction on the right side of the back, with an indentation of approximately 6 mm. The axillary pad extends from the right back, through the axilla, to the edge of the right thoracic cage, with the indentation distance decreasing to 3 mm at the anterior chest.
3) Hip: Due to the relatively thick soft tissue in the right posterior hip area, an indentation of 10-12 mm is set to offset part of the deformation; an indentation of 8 mm is applied in the torsion counteracting area.

3.4 Release Zone Design

1) Apical vertebra: The area is set on the contralateral side and slightly above the force application zone of the apical vertebra. The orthosis opening window is positioned here to enable an outward stretch of 15 mm.
2) Axillary force application zone corresponding release area: A pressure release zone is established on the contralateral side at the same horizontal level, with a stretch height of 10 mm.
3) Back release area, approximately from T5 to T12: The torsion counteracting zone of the vertebrae should be avoided. The padding thickness initially increases and then decreases, reaching a maximum of 25 mm at T12 and decreasing to a minimum of 15 mm at the hip area. The release area is illustrated in Figure 2c.

3.5 Body Shape Adjustment and Orthosis Fabrication

Raise the trunk above T6 upward by 12 mm to apply a longitudinal load to the patient; shift the trunk above T6 of the patient 12 mm to the right to make the model relatively symmetrical.

Fill in the scope of the orthosis according to the orthotic principle of the Chêneau orthosis:

Anterior part: The anterior side of the orthosis extends along the thoracic cage to the pelvis. The abdominal opening width is set at 50 mm, with the lower edge terminating 30–40 mm below the anterior superior iliac spine at the groin and the lowest point located 20 mm above the pubic symphysis.

Posterior part: The upper edge of the back is trimmed to cover the back support structure below the scapula. The lower edge extends to 1/3–1/2 of the hip height. For specific trimming ranges, refer to Figure 3.

The thickness of the orthosis is set at 3.8 mm. The method adopted during the human body model processing stage is reused to eliminate geometric errors in the boundary area of the orthosis. Regarding personalized design objectives, Liu Xiaomei [16] et al. achieved precise positioning of the scoliosis site and the application of targeted orthotic forces by 3D scanning the patient's body surface data and combining it with imaging to construct a personalized 3D model. This study has similarly achieved comparable results.

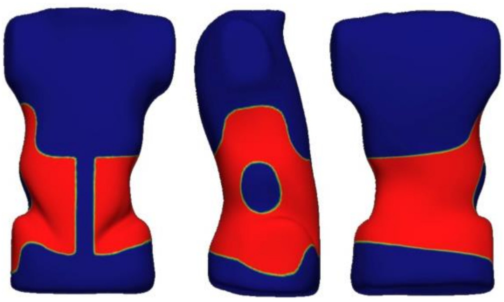

Figure 3 Cutting range of spinal orthosis

4 Finite Element Analysis (FEA) of Orthosis

4.1 Establishment of the Finite Element Model for the Orthosis

The model's surface patches are divided to provide a basis for the subsequent application of loads. Using the positions of the iliac crests and force application zones specified in the orthosis design as key references, the positions and shapes of contour lines are set, and the layout of contour lines in areas with severe curvature changes is improved. To meet the precision requirements, the minimum number of surface patches, set at 600, is used.

Before analysis, nylon with a yield strength of 75 MPa is selected as the material for the spinal orthosis [17]. The design space and non-design space are defined, with the non-design space encompassing the load application zones and fixed constraint zones. Based on the previously set contour lines, each load zone is separated from the model, and the contact mode is set to bonded contact.

Two loading conditions are established to simulate the forces acting on the orthosis under different usage scenarios: the wearing state and the state where an opening force is applied to the orthosis.

Loading Condition 1: Wearing Condition. This condition simulates the forces acting on the orthosis from the human body when the person is standing, including the three-point forces on the spine, the forces opposing vertebral torsion, and the preload at the opening, along with fixed constraints at the iliac crests on both sides. The corrective force at the apical vertebra can be determined using the following bending beam derivation formula [18]:

$$\begin{cases} E_Z \dfrac{\Delta\varphi}{\varphi}\left(\mathrm{r_c} - \mathrm{r}\right)A = R_A x - F_1\left(x - x_1\right) - F_2\left(x - x_2\right) - \dots - F_i\left(x - x_i\right)\left(0 \le x_1 < x_2 < \dots < x_i \le x\right) \\ E_Z \dfrac{\Delta\varphi}{\varphi}\left(\mathrm{r_c} - \mathrm{r}\right)A = R_B\left(l - x\right) - F_n\left(x_n - x\right) - \dots - F_{i+1}\left(x_{i+1} - x\right), \left(x \le x_{i+1} < \dots < x_\mathrm{n} \le l\right) \end{cases} \tag{1}$$

Among them, the two reaction forces R_A and R_B are determined by the following formulas:

$$\begin{cases} R_\mathrm{A} = \dfrac{F_1\left(l - x_1\right)}{l} + \dfrac{F_2\left(l - x_2\right)}{l} + \dots + \dfrac{F_n\left(l - x_n\right)}{l}, \left(x \le x_{i+1} < \dots < x_n \le l\right) \\ R_\mathrm{B} = \dfrac{F_1 x_1}{l} + \dfrac{F_2 x_2}{l} + \dots + \dfrac{F_n x_n}{l}, \left(x \le x_{i+1} < \dots < x_n \le l\right) \end{cases} \tag{2}$$

Where:

E_Z—Comprehensive elastic modulus of the spine, taken as 0.314 MPa;

$\Delta\Phi$—Orthotic correction angle, where Φ is the Cobb angle of 19°, and $\Delta\Phi$=1/2Φ;

r_c, r—Radii of the geometric central axis and neutral axis, respectively, with r_c-r=10 mm;

A—Cross-sectional area of the spine, approximated as an ellipse, with an area of approximately 1413.42 mm² measured using Mimics software;

l—Vertical distance between the upper and lower end vertebrae, taken as l=180 mm;

x_1—Optimal force application position at the apical vertebra;

F_1—Optimal magnitude of the applied force.

Since this case involves unilateral scoliosis, only the scenario with n=1 is considered. Substituting into Equations 1 and 2, the optimal magnitude of the corrective force F_1 at the apical vertebra is calculated to be 44.35 N, with the optimal force application position x_1=81.17 mm, i.e., 81.17 mm from the vertical distance of the lower end vertebra. This calculated position is essentially the same as the position determined during the orthosis design. The magnitudes of the two forces RA and RB, which form the three-point force system, are 24 N and 20 N, respectively. The magnitude of the force F_2 in the torsion counteracting zone is 70 N. When applying loads, a larger surface area is used for force application [19]. Four preload force application zones (F_3, F_4, F_5, F_6) are set at the opening, collectively bearing a total preload of 60 N, with each zone assigned a preload of 15 N, directed inward along the horizontal plane.

Loading Condition 2 focuses on simulating the mechanical characteristics during the stage of opening the orthosis during wearing. In this state, the orthosis only withstands a horizontally outward opening force of 75 N [19], uniformly distributed on both sides of the abdominal opening. In the simulation, a force of 75 N can be applied on one side, while a fixed constraint is applied on the other side, which is equivalent in simulation results. The boundary conditions for each loading condition and the loading situation of the orthosis are shown in Table 2 and Figure 4.

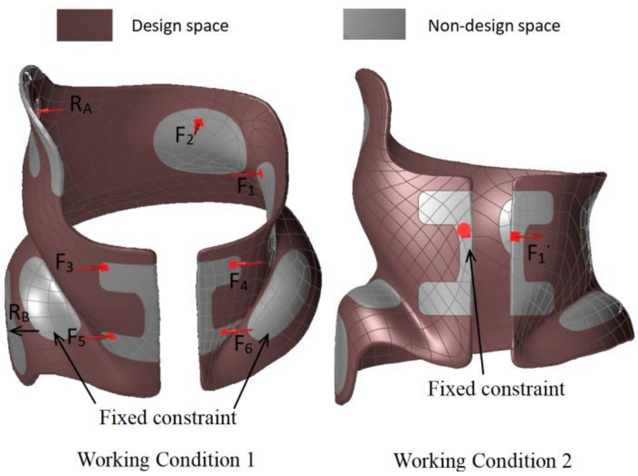

Figure 4 Constraints and Loading Conditions for Topology. Optimization

Table 2 Boundary Conditions for the Two Operating Conditions

Region	Loading Condition1 /N	Loading Condition2 /N
Apical Vertebra Region	44.35	0
Axillary Region	24	0
Hip Region	20	0
Back Region	70	0
Anterior Chest Preload Region	15	0
Left side of the opening	0	75
Right Side of the Opening	0	Fixed Constraint
Bilateral Iliac Crests	Fixed Constraint	0

4.2 Preliminary Simulation Results

Select the analysis command in the structural simulation module of Inspire to perform mechanical simulation. Set the mesh size to 2.0 mm, select both loading condition options, and the simulation analysis results are shown in Figure 5.

Nylon is classified as a brittle material, and its allowable stress is calculated using the following formula:

$$[\sigma]=\frac{\sigma_S}{S} \tag{3}$$

$[\sigma]$ — Allowable stress of the material;

σ_S — Yield strength of the material, 75 MPa;

S — Safety factor, taken as 1.5 in this case;

By substituting these values into Formula 3, the allowable stress of the material is calculated to be 50 MPa.

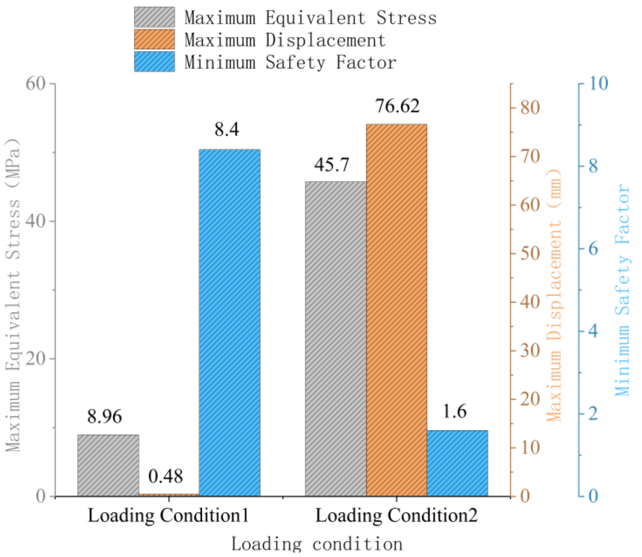

Figure 5 Simulation Result Data for the Two Operating Conditions.

Analysis of Simulation Data:

The operational intensity under Loading Condition 2 significantly exceeds that of Loading Condition 1. However, the maximum equivalent stress (45.7 MPa) remains below the allowable stress of the orthosis material, occurring at the edge of the opening window near the right posterior back region. The software indicates a minimum safety factor of 1.6, which exceeds the minimum requirement of 1.5. During wear, the maximum displacement of the orthosis is observed at the right axilla, measuring 0.48 mm, while the maximum deformation of 76.62 mm under Loading Condition 2 occurs along the opening side of the orthosis. This displacement ensures both ease of donning for the patient and compliance with strength requirements. The analysis results demonstrate that the orthosis meets strength requirements across all usage scenarios, making it suitable for topological optimization. Lian Wei et al. [20] conducted finite element analysis of the orthosis under dual loading conditions (donning and expansion), with stress results showing similar trends to this study. This validates the rationality of the research methodology and the mechanical reliability of personalized orthoses. Detailed data are provided in Table 3.

Table 3 Mechanical Performance Parameter Values of the Orthosis Under Two Operating Conditions.

parameter	Loading Condition1	Loading Condition2	Result Envelope
Maximum Displacement /mm	0.48	76.6	76.6
Minimum Safety Factor	8.4	1.6	1.6
Maximum Equivalent Stress /MPa	8.96	45.72	45.72

5 Topological Optimization Analysis

5.1 Mechanical Analysis of Optimization Results

Under the condition of maintaining the original loading scenarios unchanged, structural optimization design is carried out under four material removal rates to obtain the stress distribution states corresponding to each model. To withstand impacts arising from daily use, the minimum thickness constraint in the simulation results is set at 18 mm. The specific structural configurations, along with displacement and stress distribution characteristics, are illustrated in Figures 6 and 7.

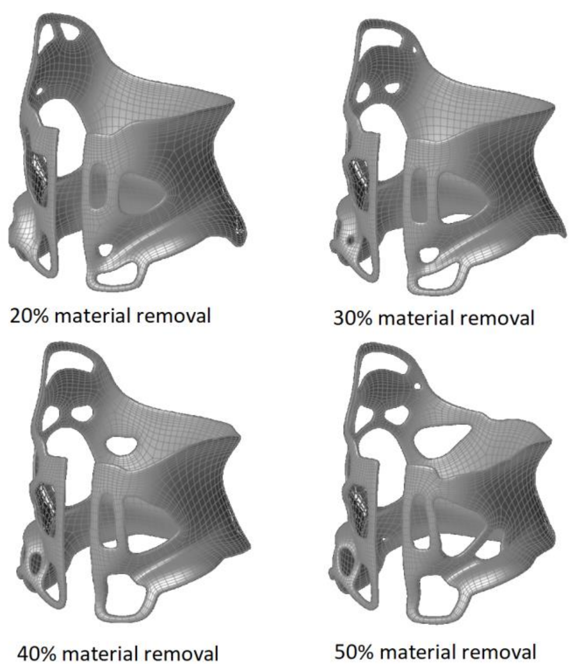

Figure 6 Topological results

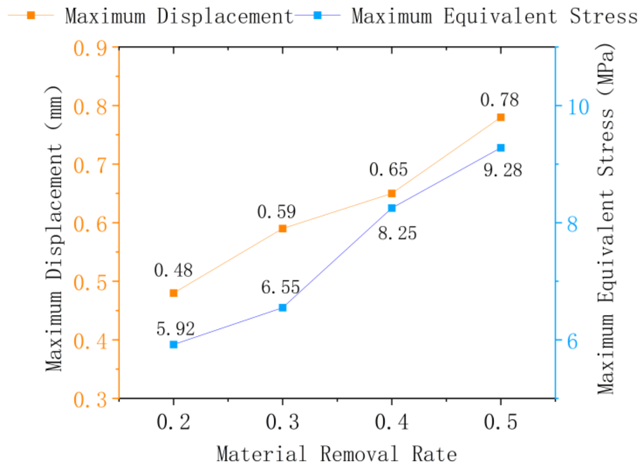

a. Condition 1

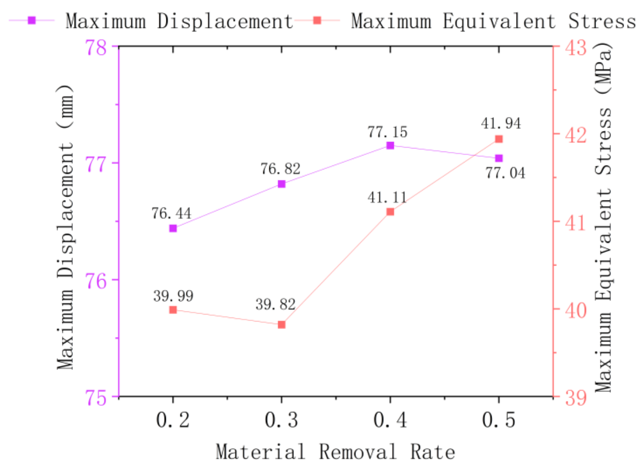

b. Condition 2

Figure 7 Constraints and Loading Conditions for Topology

The topological optimization results indicate that with the gradual increase in the material removal rate, the hollowed-out areas in the left and right anterior abdominal regions expand continuously. Meanwhile, a material reduction trend is also observed along the upper and lower edges of the dorsal section. Simultaneously, multiple small voids form within the model interior. Notably, the left iliac crest and its surrounding regions exhibit the most pronounced changes, with material volume decreasing in tandem with the reduction of material in the lower dorsal area.

Under all operational conditions, the maximum equivalent stress of the orthosis remains below the material's yield strength. In Condition 1, stress values across the entire domain remain below 10 MPa, indicating a generally low-stress state. Under Condition 2, the maximum stress initially decreases before subsequently increasing. This trend is analyzed as follows: topological optimization has, to a certain extent, improved the model's mechanical performance by mitigating stress concentration phenomena. However, the subsequent stress increase stems from the elevated material removal during optimization, which reduces overall structural stiffness and elevates stress under equivalent loading conditions—though remaining below the material's allowable stress limit of 50 MPa.

The displacement trends of the orthosis under dual operational conditions exhibit a positive correlation with the material removal rate, sharing the same mechanistic explanation as the stress increase phenomenon. In Condition 1, displacements in the orthotic correction zones do not exceed 30% of the orthosis thickness [21] (i.e., 1.14 mm), meeting stiffness requirements. Condition 2 demonstrates a maximum displacement of 77 mm, consistent with preliminary simulation findings.

For the 50% material removal rate scenario, the orthosis experiences a peak stress of 41.94 MPa. While this value maintains a safety margin relative to the 50 MPa allowable limit, further simulations reveal that increasing the material removal rate beyond this point leads to simulation distortion and model discontinuity, preventing the software from generating valid results. In comparison, a material retention rate corresponding to a weight reduction effect that is less than 50% indicates insufficient weight-loss efficacy. After comprehensive evaluation, the scheme with "a 50% material removal rate" is determined to be the relatively optimal one among the four options.

5.2 Secondary Topological Optimization and Result Analysis

Analysis of the Results:From the perspective of lightweight design objectives, the left iliac crest region, which is either non-design space or has potential for further weight reduction, can be considered for modification. From a biomechanical standpoint, the force-application zone at the apex vertebra is in close spatial proximity to the iliac crest region. Moreover, the apex vertebra force-application zone can provide structural support and fixation for the orthosis through its inherent mechanical transmission properties. Under these conditions, removing or reducing material in this region will not adversely affect the overall force equilibrium or wearing stability of the orthosis. during preliminary mechanical simulations, stresses in this region remained consistently below 10 MPa under both operational conditions, indicating it is a non-critical load-bearing area that exhibits high material removability in topological optimization.

Based on this analysis, the left iliac crest region is redefined as design space while keeping other regions unchanged. Loading conditions remain identical to those in the secondary topological optimization. Two comparative schemes are established: Scheme 1 ("Left iliac crest defined as design space") and Scheme 2 ("50% material removal rate"). These schemes are analyzed to observe material distribution patterns and mechanical response characteristics in the targeted region. The topological optimization results, stress contour plots, and key parameters are presented in Figure 8 and Table 4.

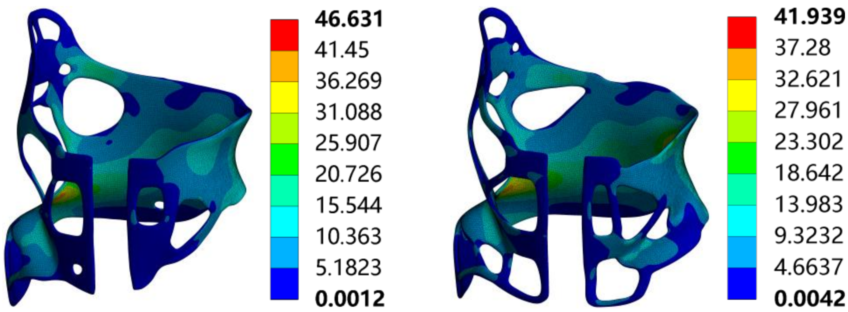

a. Scheme 1 b. Scheme 2

Figure 8 Comparison of Topological Results and Stress Contour Maps Between the Two Schemes

Table 4 Comparison of Key Parameters Between the Two Schemes

	Maximum Displacement in the Orthotic Region /mm	**Maximum Equivalent Stress /MPa**	**Mass /kg**
Scheme 1	0.74	46.63	0.346
Scheme 2	0.78	41.94	0.371
Original Model	0.48	45.70	0.592

1) Topological Shape: In Scheme One, the volume of material removed from the left iliac crest and its adjacent areas is significantly larger than that in Scheme Two, while there are no noticeable changes in material distribution across the remaining regions of the model.
2) Displacement Analysis: The deformation in the orthotic regions of both schemes is below the threshold specified in the orthosis failure criterion, which mandates that "the maximum displacement should be less than 30% of the thickness (1.14 mm)", thereby complying with the structural stiffness design specifications.
3) Mechanical Performance: The maximum stress in Scheme Two registers at 41.94 MPa, with a model mass of 0.371 kg. In Scheme One, the maximum stress around the left iliac crest is 14.52 MPa, comparable to that of the original model and well below the material's allowable stress. This demonstrates that optimizing the area around the left iliac crest does not lead to a sudden spike in stress in this region, thus validating the rationality of the design approach of "eliminating non-design space in this area" from a mechanical performance standpoint. After optimization, the overall maximum stress in Scheme One reaches 46.63 MPa, and the model mass is reduced to 0.346 kg. While achieving a further 6.7% reduction in model mass, Scheme One only results in an 8% increase in maximum stress, with the final stress value remaining within the material's allowable stress limits. These findings are consistent with the research by Julien Clin [22] et al., whose method of comparing orthoses with varying material removal rates and the resulting force patterns after weight reduction aligns with this study. Slawomir Grycuk [23] et al. identified the force flow by mapping the paths of maximum principal stress, clarifying that regions that are not core force-bearing areas and not on force transmission paths can be prioritized for material removal, which is in line with the optimization direction of "eliminating non-design space around the left iliac crest".

From the multi-faceted verification of the rationality of Scheme One, it is evident that in terms of mechanical stability, the apical vertebra region can substitute for the left iliac crest, right iliac crest, and armpit to ensure the orthosis's stability. In terms of mechanical performance, the simulation results corroborate the scheme's rationality. The aforementioned two outcomes provide theoretical support for the scheme of "eliminating non-design space around the left iliac crest". Consequently, Scheme One is selected as the final topological optimization scheme, achieving a final mass reduction of 41.6%. Based on this optimal scheme, subsequent work will involve re-modeling the orthosis using the shape of the orthosis in Scheme One as a reference, defining an outer contour consistent with the optimal scheme to enhance the model's aesthetic appeal and regularity.

6 Conclusions

In response to the issue of poor patient tolerance caused by the bulkiness of traditional spinal scoliosis orthoses, this study took a 14-year-old patient with thoracolumbar single-curve scoliosis accompanied by kyphosis as the specific research subject. By employing 3D scanning, reverse modeling, and X-ray model registration, an initial orthosis model that closely conformed to the individual's torso characteristics was constructed. With the objective of achieving "lightweight design while ensuring mechanical performance," the study first utilized finite element analysis to simulate the stress and deformation patterns under two working conditions: wearing and opening. From four material removal schemes, the optimal initial scheme of "50% material removal" was selected. Subsequently, a secondary topological optimization was conducted, focusing on the non-critical stress area of the left iliac crest. Ultimately, the orthosis achieved a total weight reduction of 41.6% (from 0.592 kg to 0.346 kg), with both the maximum stress (46.63 MPa) and maximum deformation (0.74 mm) meeting the design requirements.

The lightweight design process employed in this study provides a technical reference for the design of similar orthoses and can directly improve patient comfort during wear. Subsequent verification of its practical application effectiveness can be conducted through 3D printing and clinical testing.

References

[1] Del Prete C M, Tarantino D, Viva M G, et al. Spinal orthosis in adolescent idiopathic scoliosis: an overview of the braces provided by the National Health Service in Italy [J]. Medicina, 2023, 60(1): 3. https://doi.org/10.3390/medicina60010003

[2] Jing W, Jin Z, Rui X, et al. Measurement of scoliosis Cobb angle by end vertebra tilt angle method. [J]. Journal of orthopaedic surgery and research, 2018, 13(1): 223. https://doi.org/10.1186/s13018-018-0928-5

[3] Ogilvie J. Adolescent idiopathic scoliosis and genetic testing [J]. Current opinion in pediatrics, 2010, 22(1): 67-70. https://doi.org/10.1097/MOP.0b013e32833419ac

[4] Simhon M E, Fields M W, Grimes K E, et al. Completion of a formal physiotherapeutic scoliosis-specific exercise training program for adolescent idiopathic scoliosis increases patient compliance to home exercise programs [J]. Spine Deformity, 2021, 9(3): 691-696. https://doi.org/10.1007/s43390-020-00253-8

[5] Minsk MK, Venuti KD, Daumit GL, Sponseller PD. Effectiveness of the Rigo Chˆeneau versus Boston-style orthoses for adolescent idiopathic scoliosis: a retrospective study [J]. Scoliosis and Spinal Disorders 2017; 12(1). https://doi.org/10.1186/s13013-017-0117-z

[6] Weinstein SL, Dolan LA, Wright JG, Dobbs MB. Effects of Bracing in Adolescents with Idiopathic Scoliosis [J]. N Engl J Med 2013; 1512-1521. https://doi.org/10.1056/nejmoa1307337

[7] Wei W, Zhang T, Huang Z, et al. Finite element analysis in brace treatment on adolescent idiopathic scoliosis [J]. Medical & Biological Engineering & Computing, 2022, 60(4): 907-920. https://doi.org/10.1007/s11517-022-02524-0

[8] IASON ROSSETOS, CHARIS J. GANTES, GEORGE KAZAKIS, et al. Numerical Modeling and Nonlinear Finite Element Analysis of Conventional and 3D-Printed Spinal Braces [J]. Applied Sciences, 2024, 14(5). https://doi.org/10.3390/app14051735

[9] Liao Y C, Feng C K, Tsai M W, et al. Shape modification of the Boston brace using a finite-element method with topology optimization [J]. Spine, 2007, 32(26): 3014-3019. https://doi.org/10.1097/BRS.0b013e31815cda9c

[10] Cobetto N, Aubin C E, Parent S, et al. Effectiveness of braces designed using computer-aided design and manufacturing (CAD/CAM) and finite element simulation compared to CAD/CAM only for the conservative treatment of adolescent idiopathic scoliosis: a prospective randomized controlled trial [J]. European spine journal, 2016, 25(10): 3056-3064. https://doi.org/10.1007/s00586-016-4434-3

[11] Tz-How H, Chi-Kung F, Yih-Wen G, et al. Optimization design of thumbspica splint using finite element method. [J]. Medical & biological engineering & computing, 2006, 44(12): 1105-11. https://doi.org/10.1007/s11517-006-0131-4

[12] F S K, A M Z, L T. Lightweight design of Knee-Ankle-Foot Orthotic Devices using Voronoi patterns for Additive Manufacturing [J]. Journal of Physics: Conference Series, 2023, 2643(1). https://doi.org/10.1088/1742-6596/2643/1/012007

[13] Du Y, Li Y, Wu Z, et al. Research on filtering and measurement algorithms based on human point cloud data [J]. International Journal of Intelligent Systems, 2022, 37(12): 12252-12266. https://doi.org/10.1002/int.23085

[14] Schlösser T P C, Van Stralen M, Brink R C, et al. Three-dimensional characterization of torsion and asymmetry of the intervertebral discs versus vertebral bodies in adolescent idiopathic scoliosis [J]. Spine (Phila Pa 1976).39: E1159-1166. (2014). https://doi.org/10.1097/brs.0000000000000467

[15] Majdouline Y, Aubin C E, Robitaille M, et al. Scoliosis correction objectives in adolescent idiopathic scoliosis [J]. Journal of Pediatric Orthopaedics, 2007, 27(7): 775-781. https://doi.org/10.1097/BPO.0b013e31815588d8

[16] Liu Xiaomei, Zhou Yong, Wang Yanyang, et al. Application of 3D printing technology combined with computer-aided design in the manufacture of scoliosis orthosis [J]. Chinese medical equipment journal, 2023, 44(5): 74-80. https://doi.org/10.19745/j.1003-8868.2023098

[17] Lu D, Li T, Yu W, et al. Expert consensus on the design, manufacture, materials, and clinical application of customized three-dimensional printing scoliosis orthosis [J]. Digital Medicine, 2022, 8: 2. https://doi.org/10.4103/ digm.digm_34_21

[18] Zhang, Y. F., Guo, H. W., Lü, M., et al. (2025). Calculation and analysis of scoliosis correction force [J]. Machinery Design & Manufacture, (07), 30-34. https://doi.org/10.19356/j.cnki.1001-3997.20241227.058

[19] Ren, D., Zhu, Y., Lei, L., & Wang, Y. R. (2022). Finite element analysis of the effect of orthopedic force applied to rib force - application areas on the displacement and rotation angle of the thoracic vertebrae [J]. Chinese Journal of Tissue Engineering Research, 26(18), 2812-2816. https://doi.org/10.12307/ 2022.686

[20] Lian, W., Wang, H. S., & Yu, J. (2021). Local optimization design of 3D-printed scoliosis orthosis based on finite element analysis [J]. Journal of Medical Biomechanics, 36(06), 855-861. https://doi.org/10.16156/j.1004-7220.2021.06.004

[21] Curfs I, Rooij V W, Senden R, et al. Evaluating the Immobilization Effect of Spinal Orthoses Using Sensor-Based Motion Analysis [J]. Journal of Prosthetics and Orthotics, 2016, 28(1): 23-29. https://doi.org/10.1097/JPO.0000000000000085

[22] Clin J, Aubin C E, Parent S, et al. Comparison of the biomechanical 3D efficiency of different brace designs for the treatment of scoliosis using a finite element model [J]. European Spine Journal, 2010, 19(7): 1169-1178. https://doi.org/10.3233/bme-2010-0639

[23] Grycuk S, Mrozek P. Finite Element Model of Scoliosis Brace with Increased Utility Characteristics [J]. Applied Sciences, 2023, 13(24): 13273. https://doi.org/10.3390/app132413273.2022